Bidirectional Reflectance Spectroscopy

5. The Coherent Backscatter Opposition Effect and Anisotropic Scattering

Bruce Hapke

Department of Geology and Planetary Science, University of Pittsburgh, Pittsburgh, Pennsylvania 15260
E-mail: hapke@pitt.edu

A model published previously by the author that describes light scattering from particulate media is modified to include several improvements: (1) a better approximation to the Ambartsumian–Chandrasekhar H-functions that is especially important for particles with single scattering albedos close to 1.00, (2) increased accuracy for anisotropically scattering particles, and (3) incorporation of coherent backscattering. The goal of the original model of being analytic and mathematically tractable is preserved. No new parameters are introduced by the first and second modifications; however, the third unavoidably adds two new parameters: the amplitude and width of the coherent backscatter opposition effect. Several examples are given in which the results of calculations using the original and new models are compared with exact numerical computations.

It is shown that a medium composed of complex particles that are large compared to the wavelength can have a coherent backscatter opposition effect (CBOE) that is broad enough to be readily observable. The CBOE multiplies the entire reflectance and not just the multiply scattered component, so that a low-albedo medium, such as lunar regolith, can have a strong CBOE. © 2002 Elsevier Science (USA)

1. INTRODUCTION

Even though the wide availability of high-speed desk-top computers allows exact numerical solutions of the radiative transfer equation to be conveniently evaluated, there are still many times when an approximate analytic solution is useful. These include analyses of large data sets, inversion of solutions to estimate optical parameters, and situations in which high absolute accuracy is not necessary. The latter is frequently encountered in reflectance measurements of particulate media such as planetary regoliths (Hapke 1999). The author has put forward such an approximate model in several publications (Hapke 1981, 1984, 1986, 1993).

However, the usefulness of the original model was limited because of several deficiencies: (1) Even if the opposition effect is ignored, the calculated absolute reflectance can be incorrect by as much as 16% when the single scattering albedo is close to 1.00. (2) The absolute accuracy is low at certain angles when the particles of the medium are highly anisotropc scat-

terers. (3) In the original model the entire opposition effect is assumed to be caused by shadow-hiding and to reside only in the single-scattering reflectance term; however, since the model was published it has been recognized that a large fraction of the opposition effect is caused by coherent backscatter (Kuga and Ishimaru 1984, Shkuratov 1988, Muinonen 1990, Hapke 1990, Mischenko and Dlugach 1992, Hapke *et al.* 1993, 1998, Helfenstein *et al.* 1997, Nelson *et al.* 1998, 2000), to which multiple scattering makes a major contribution. It is the purpose of this paper to improve the original model by partially correcting these deficiencies, while keeping the desirable goal of remaining analytic, albeit at the expense of a modest increase in complexity. The opposition effect is discussed in some detail in order to provide a framework for the expression chosen to describe coherent backscattering. As in the original model, it is assumed that the particles are large compared to the wavelength, irregular in shape, and randomly positioned and oriented.

2. THE ISOTROPIC MULTIPLE-SCATTERING APPROXIMATION

In the original model (Hapke 1981, 1993) the single-scattering term is calculated exactly, while the multiple-scattering contribution is approximated by the two-stream solution to the equation of radiative transfer for isotropic scatterers, even when the scattering is anisotropic. Therefore, this model will be refered to as the isotropic multiple-scattering approximation (IMSA). In the IMSA model the bidirectional reflectance of a planar, semi-infinite, particulate medium illuminated by collimated light from zenith angle i and observed at zenith angle e and phase angle g is written

$$r(i, e, g) = \frac{w}{4\pi} \frac{\mu_o}{\mu_o + \mu} [p(g) + H(\mu_o)H(\mu) - 1], \quad (1)$$

where $p(g)$ is the single-particle angular scattering function, normalized so that

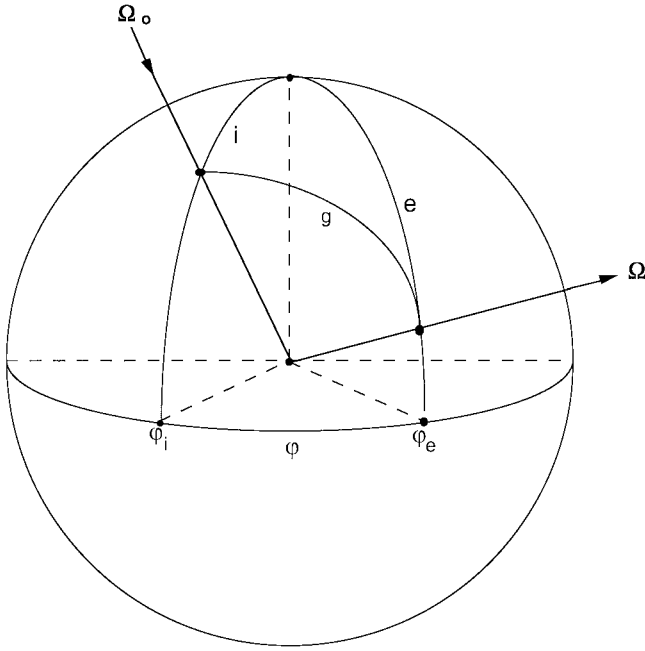$$\frac{1}{4\pi} \int_{4\pi} p(g) \, d\Omega = 1,$$

523

FIG. 1. Diagram of angles used in this paper.

w is the single-scattering albedo, $\mu_o = \cos i$, $\mu = \cos e$, and $d\Omega$ is an increment of solid angle; the H-functions are approximated by

$$H(x) = \frac{1 + 2x}{1 + 2\gamma x}, \qquad (2)$$

where $\gamma = \sqrt{1 - w}$. The various angles are illustrated in Fig. 1. Equation (1) does not include the shadow-hiding opposition effect and the effects of large-scale roughness. These will be discussed later.

When the scatterers are isotropic, $p(g) = 1$, and the reflectance is

$$r(i, e, g) = \frac{w}{4\pi} \frac{\mu_o}{\mu_o + \mu} H(\mu_o) H(\mu). \qquad (3)$$

3. THE INVARIANCE EQUATION

Instead of solving the radiative transfer equation the principle of invariance will be used to derive the improved model for the bidirectional reflectance. This principle (also known as invariant embedding) states that the reflectance of a semi-infinite, particulate medium does not change if an optically thin layer of identical particles is placed on top of it. Mathematically, the sum of the first-order terms in the optical thickness of the layer is zero. This leads (Ambartsumian 1958, Chandrasekar 1960, Sobolev 1975, Hapke 1993) to the nonlinear integral equation

for the reflectance

$$\left(\frac{1}{\mu_o} + \frac{1}{\mu} \right) r(\Omega_o, \Omega)$$

$$= \frac{w}{4\pi} \left[\frac{1}{\mu} p(\Omega_o, \Omega) + \int_{\substack{\Omega'_o = \text{lower} \\ \text{hemisphere}}} p(\Omega_o, \Omega'_o) \frac{r(\Omega'_o, \Omega)}{\mu'_o} \, d\Omega'_o \right.$$

$$+ \int_{\substack{\Omega' = \text{upper} \\ \text{hemisphere}}} \frac{r(\Omega_o, \Omega')}{\mu} p(\Omega', \Omega) \, d\Omega'$$

$$\left. + \int_{\substack{\Omega' = \text{upper} \\ \text{hemisphere}}} \int_{\substack{\Omega'_o = \text{lower} \\ \text{hemisphere}}} r(\Omega_o, \Omega') p(\Omega', \Omega'_o) \frac{r(\Omega'_o, \Omega)}{\mu'_o} \, d\Omega'_o \, d\Omega' \right],$$

$$(4)$$

where $r(\Omega_o, \Omega)$ is the bidirectional reflectance for scattering light incident from direction $\Omega_o = (i, \varphi_i)$ into direction $\Omega = (e, \varphi_e)$, $p(\Omega_o, \Omega) = p(g)$ is the single-particle function for scattering light incident from direction Ω_o into direction Ω, and φ_i and φ_e are azimuth angles. Primed quantities are analgously defined. The directions Ω_o and Ω are separated by phase angle g and azimuth angle $\varphi = \varphi_e - \varphi_i$. The various angles are related by

$$\cos g = \cos i \cos e + \sin i \sin e \cos \varphi. \qquad (5)$$

Because the derivation of Eq. (4) has been published in several places it will not be repeated here. The term on the left in this equation describes light that has been partly extinguished by passage through the added layer on the way in, scattered from the original medium, and partly extinguished by the layer again on the way out. This light must be equal to the light added by the layer described by the right-hand side. The first term inside the square brackets on the right describes the light that is scattered directly by particles in the layer from the source into the detector. The second term is light scattered from the layer down to the original medium and then into the detector. The third term is light that is scattered from the original medium toward the layer and then into the detector. The last term desribes light scattered from the original medium to the layer, then back to the medium, and finally to the detector. It should be noted that this formulation, like the derivation based on radiative transfer theory, does not include either shadow-hiding or coherent backscatter, which must be added later in an *ad hoc* manner.

Let

$$L(\Omega_o, \Omega) = \frac{4\pi}{w} \frac{\mu_o + \mu}{\mu_o} r(\Omega_o, \Omega). \qquad (6)$$

Substituting this into Eq. (4) gives a nonlinear equation,

$$L(\Omega_o, \Omega) = p(\Omega_o, \Omega) + \frac{w}{4\pi}\mu \int\limits_{\Omega_o'} p(\Omega_o, \Omega_o')\frac{L(\Omega_o', \Omega)}{\mu_o' + \mu}\, d\Omega_o'$$

$$+ \frac{w}{4\pi}\mu_o \int\limits_{\Omega'} \frac{L(\Omega_o, \Omega')}{\mu_o + \mu'} p(\Omega', \Omega)\, d\Omega' + \left(\frac{w}{4\pi}\right)^2 \mu_o\mu$$

$$\times \int\limits_{\Omega'} \int\limits_{\Omega_o'} \frac{L(\Omega_o, \Omega')}{\mu_o + \mu'} p(\Omega', \Omega_o')\frac{L(\Omega_o', \Omega)}{\mu_o' + \mu}\, d\Omega_o'\, d\Omega'.$$

$$(7)$$

As first shown by Ambartsumian (1958), in the special case of isotropic scatterers, $p(g) = 1$, L is independent of azimuth and is a function only of μ_o and μ, so that the fourth term on the right may be factored into two independent integrals. Then Eq. (6) becomes

$$L(\mu_o, \mu)$$

$$= 1 + \frac{w}{2}\mu \int\limits_0^1 \frac{L(\mu_o', \mu)}{\mu_o' + \mu}\, d\mu_o' + \frac{w}{2}\mu_o \int\limits_0^1 \frac{L(\mu_o, \mu')}{\mu_o + \mu'}\, d\mu'$$

$$+ \left[\frac{w}{2}\mu_o \int\limits_0^1 \frac{L(\mu_o, \mu')}{\mu_o + \mu'}\, d\mu'\right]\left[\frac{w}{2}\mu \int\limits_0^1 \frac{L(\mu_o', \mu)}{\mu_o' + \mu}\, d\mu_o'\right]$$

$$= \left[1 + \frac{w}{2}\mu_o \int\limits_0^1 \frac{L(\mu_o, \mu')}{\mu_o + \mu'}\, d\mu'\right]\left[1 + \frac{w}{2}\mu \int\limits_0^1 \frac{L(\mu_o', \mu)}{\mu_o' + \mu}\, d\mu_o'\right].$$

Thus, L consists of the product of two identical functions, one dependent only on μ_o and one only on μ, given by

$$L(\mu_o, \mu) = H(\mu_o)H(\mu), \qquad (8)$$

where the Ambartsumian–Chandrasekhar H-functions for isotropic scatterers are the solutions of the integral equation

$$H(x) = 1 + \frac{w}{2}xH(x)\int\limits_0^1 \frac{H(x')}{x + x'}\, dx', \qquad (9)$$

and x can be either μ_o or μ. Hence, the reflectance is

$$r(i, e, g) = r(\mu_o, \mu) = \frac{w}{4\pi}\frac{\mu_o}{\mu_o + \mu}H(\mu_o)H(\mu), \qquad (10)$$

which may be compared with Eq. (3). The H-functions defined in Eq. (2) used in the IMSA model are analytic approximations to the exact H-functions defined by Eq. (9).

4. IMPROVEMENT 1: A MORE ACCURATE EXPRESSION FOR THE H-FUNCTIONS

Equation (9) may be rearranged to give

$$H(x) = \left[1 - \frac{w}{2}x \int\limits_0^1 \frac{H(x')}{x + x'}\, dx'\right]^{-1}. \qquad (11)$$

Now, the H-functions are almost linear fuctions of x. Hence, a first-order approximation to them may be written as $H(w, x) \approx C + Dx$. Since $H(w, 0) = 1$, choose $C = 1$. By direct integration of Eq. (9) the mean value of the H-function is readily shown to be (Chandrasekhar 1960, Hapke 1993)

$$\langle H(w) \rangle = \int\limits_0^1 H(x)\, dx = \frac{2}{1 + \gamma}.$$

Requiring the mean value of the linear approximation to have this value gives $D = 2r_o$, where

$$r_o = \frac{1 - \gamma}{1 + \gamma}. \qquad (12)$$

By inserting the linear approximation into (11), the integration is readily carried out, giving the second-order approximation

$$H(x) \approx \left[1 - wx\left(r_0 + \frac{1 - 2r_ox}{2}\ln\frac{1 + x}{x}\right)\right]^{-1}. \qquad (13)$$

Chandrasekhar (1960) has published tables of H-functions numerically evaluated from Eq. (9) for several values of w and x. The relative difference between the approximate and exact values are shown in Fig. 2 for both the IMSA [Eq. (2)] and improved
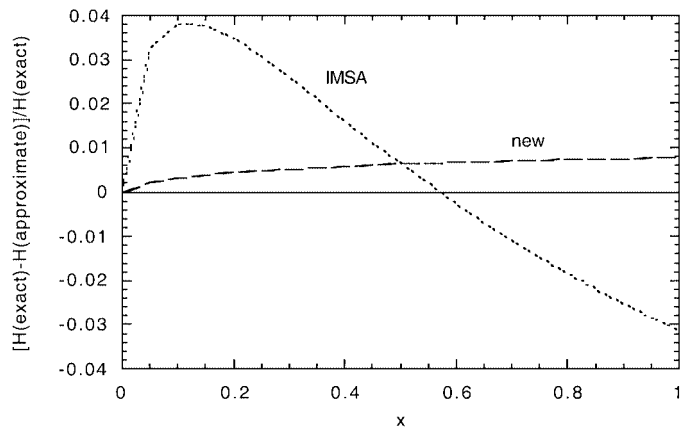

FIG. 2. Relative difference between the approximate expressions and the exact values of the H-function for isotropic scatterers plotted against the argument of the H-function.

[Eq. (13)] approximations for the case of $w = 1$. The improved expression is seen to be accurate to better than 1% everywhere, which is adequate in most situations. The relative differences are smaller for $w < 1$.

5. IMPROVEMENT 2: A MORE ACCURATE MULTIPLE-SCATTERING TERM FOR ANISOTROPIC SCATTERERS

Derivation

To obtain a more accurate, yet analytic, expression for the multiple-scattering term when the particles do not scatter isotropically, two approximations are made in the integrands in Eq. (7). (i) The particle angular scattering functions are replaced by their averages over the range of integration and taken out from under the integral. (ii) The L-functions are replaced by the expressions for isotropic scatterers, Eq. (8) in the integrals. Then the integrands are independent of azimuth and the invariance equation becomes

$$
L(\Omega_o, \Omega) \approx p(\Omega_o, \Omega) + P(\mu_o)\frac{w}{2}\mu H(\mu) \int_0^1 \frac{H(\mu_o')}{\mu_o' + \mu} d\mu_o'
$$

$$
+ P(\mu)\frac{w}{2}\mu_o H(\mu_o) \int_0^1 \frac{H(\mu')}{\mu' + \mu_o} d\mu'
$$

$$
+ \mathcal{P}\left[\frac{w}{2}\mu_o H(\mu_o) \int_0^1 \frac{H(\mu')}{\mu' + \mu_o} d\mu'\right]
$$

$$
\times \left[\frac{w}{2}\mu H(\mu_o) \int_0^1 \frac{H(\mu_o')}{\mu_o' + \mu} d\mu_o'\right], \quad (14)
$$

where $P(\mu_o)$, $P(\mu)$, and $\mathcal{P}$ are defined as follows:

$P(\mu_o)$ is the average radiance scattered into the lower hemisphere by a particle illuminated from a direction making an angle i with the vertical,

$$
P(\mu_o) = \frac{1}{2\pi} \int_{e'=\pi/2}^{\pi} \int_{\varphi'=0}^{2\pi} p(g') \sin e' \, de' \, d\varphi'. \quad (15)
$$

$P(\mu)$ is the radiance scattered by a particle into a direction in the upper hemisphere that makes an angle e with the vertical when uniformly illuminated from the entire lower hemisphere. Since photons can travel in either direction along a ray path, $P(\mu)$ has the same functional dependence on μ as $P(\mu_o)$ does on μ_o.

$\mathcal{P}$ is the average intensity scattered back into the entire lower hemisphere by a particle uniformly illuminated from the entire lower hemisphere,

$$
\mathcal{P} = \frac{1}{(2\pi)^2} \int_{i'=0}^{\pi/2} \int_{\varphi_i'=0}^{2\pi} \int_{e'=0}^{\pi/2} \int_{\varphi_e'=0}^{2\pi} p(g') \sin e' \, de' \, d\varphi_e' \, \sin i' \, di' \, d\varphi_i'.
$$

$$
(16)
$$

With these approximations and using Eq. (9), Eq. (14) becomes

$$
L(\Omega_o, \Omega) = L(i, e, g) = p(g) + M(\mu_o, \mu),
$$

where

$$
M(\mu_o, \mu) = P(\mu_o)[H(\mu) - 1] + P(\mu)[H(\mu_o) - 1]
$$
$$
+ \mathcal{P}[H(\mu) - 1][H(\mu_o) - 1], \quad (17)
$$

so that, from Eq. (6),

$$
r(i, e, g) = \frac{w}{4\pi} \frac{\mu_o}{\mu_o + \mu}[p(g) + M(\mu_o, \mu)]. \quad (18)
$$

Equation (17) for $M(\mu_o, \mu)$ is the new model for multiple scattering. Single scattering is described exactly by $p(g)$ in (18). As will be demonstrated below, the accuracy of the multiple-scattering term is considerably improved over the IMSA model, especially if Eq. (13) is used to evaluate the H-functions.

Evaluation for a Legendre Polynomial Expansion of $p(g)$

The coefficients in the improved model will be evaluated for the general case where $p(g)$ is expressed as an infinite sum of Legendre polynomials $P_n(\cos g)$:

$$
p(g) = 1 + \sum_{n=1}^{\infty} b_n P_n(\cos g). \quad (19)
$$

Properties of the Legendre polynomials are given in the mathematical literature, e.g., Jahnke and Emde (1945).

The addition theorem for Legendre polynomials states that

$$
P_n(\cos g) = P_n(\cos i)P_n(\cos e) + 2\sum_{m=1}^{n} \frac{(n-m)!}{(n+m)!} P_{nm}(\cos i)
$$
$$
\times P_{nm}(\cos e)\cos m\varphi, \quad (20)
$$

where the P_{nm} are the associated Legendre polynomials. When Eqs. (19) and (20) are inserted into (15), the integral of $\cos m\varphi$ over azimuth vanishes, giving

$$
P(\mu_o) = \frac{1}{2\pi} \int_{e'=\pi/2}^{\pi} \int_{\varphi'=0}^{2\pi} \left[1 + \sum_{n=1}^{\infty} b_n P_n(\cos i)P_n(\cos e')\right]
$$
$$
\times \sin e' \, de' \, d\varphi'
$$
$$
= 1 + \sum_{n=1}^{\infty} b_n P_n(\mu_o) \int_{x'=-1}^{0} P_n(\mu') \, d\mu', \quad (21)
$$

where $\mu' = \cos e'$. Using the recurrence relation

$$P_n(\mu') = \frac{1}{2\pi}\left[\frac{dP_{n+1}(\mu')}{d\mu'} - \frac{dP_{n-1}(\mu')}{d\mu'}\right]$$

gives

$$P(\mu_{\mathrm{o}}) = 1 + \sum_{n=1}^{\infty}\frac{b_n P_n(\cos i)}{2n+1}\{[P_{n+1}(0) - P_{n-1}(0)]$$
$$- [P_{n+1}(-1) - P_{n-1}(-1)]\}. \tag{22}$$

Now, $P_n(-1) = (-1)^n P_n(+1)$, $P_n(1) = 1$, $P_n(0) = 0$ if n is odd, and

$$P_n(0) = \frac{(-1)^{n/2}}{n+1}\frac{1\cdot 3\cdot 5\cdots(n+1)}{2\cdot 4\cdot 6\cdots n}\qquad\text{if }n\text{ is even.}$$

Using these values, Eq. (22) can be evaluated. Equation (16) for $\mathcal{P}$ can be evaluated in a similar manner. The final results, after a little algebra, are

$$P(\mu_{\mathrm{o}}) = 1 + \sum_{n=1}^{\infty} A_n b_n P_n(\mu_{\mathrm{o}}), \tag{23}$$

$$P(\mu) = 1 + \sum_{n=1}^{\infty} A_n b_n P_n(\mu), \tag{24}$$

$$\mathcal{P} = 1 - \sum_{n=1}^{\infty} A_n^2 b_n, \tag{25}$$

where

$$A_n = 0 \qquad\qquad\text{if }n = \text{even}, \tag{26}$$

$$A_n = \frac{(-1)^{\frac{n+1}{2}}}{n}\frac{1\cdot 3\cdot 5\cdots n}{2\cdot 4\cdot 6\cdots(n+1)}\qquad\text{if }n = \text{odd}. \tag{27}$$

The coefficients A_n and A_n^2 are listed to 15th order in Table I. Several examples are given in the following sections.

TABLE I
Legendre Scattering Function Coefficients

n	A_n	A_n^2
1	−0.5000	0.2500
3	0.1250	0.0156
5	−0.0625	0.00391
7	0.0391	0.00153
9	−0.0273	0.000748
11	0.0205	0.000421
13	−0.0161	0.000259
15	0.0131	0.000172

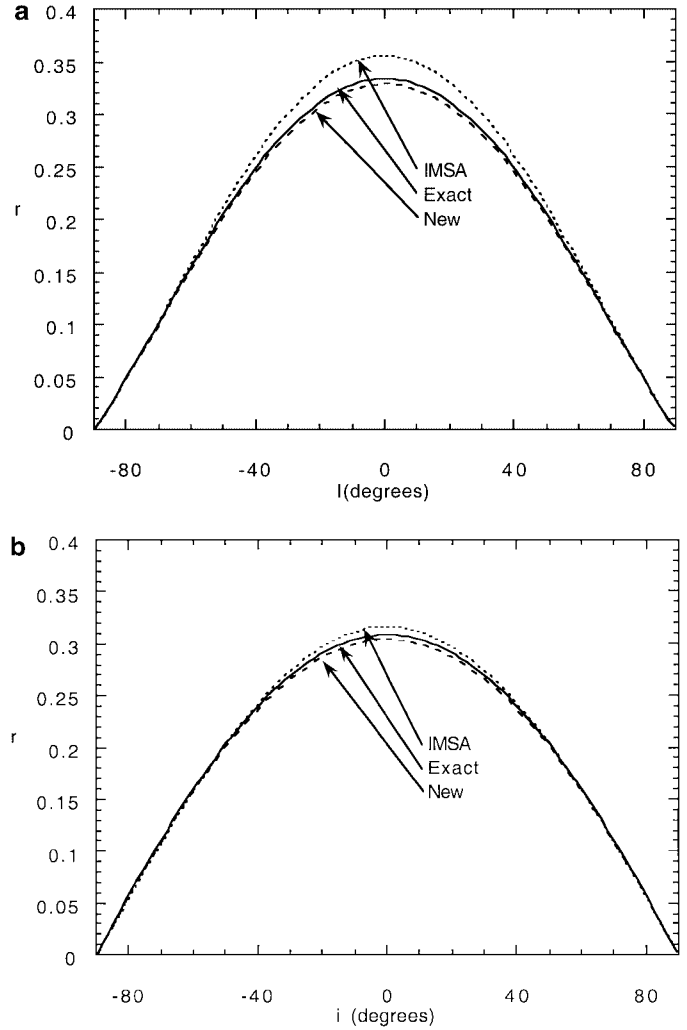*Note.* For n = even, $A_n = A_n^2 = 0$.

FIG. 3. Reflectance in the principal plane as a function of angle of incidence of a medium of isotropic scatterers [$p(g) = 1$] with $w = 1.00$ calculated using the IMSA model, the new analytic model derived in this paper, and the exact values calculated numerically; negative values of i indicate that the source is on the opposite side of the normal from the detector; (a) $e = 0°$; (b) $e = 60°$.

Isotropic Scatterers

For isotropic scatterers,

$$p(g) = 1.$$

Then $P(i) = P(e) = \mathcal{P} = 1$, and Eq. (18) is the same as Eq. (10). This case is plotted in Fig. 3, which shows the reflectance in the principal plane as a function of i for the case of $w = 1$ and $e = 0°$ and $60°$. The improved model and the IMSA model are compared with an exact numerical calculation using the tabulted data from Chandrasekhar (1960) and demonstrates the greater accuracy of Eq. (13) over Eq. (2).

First-Order Legendre Polynomial

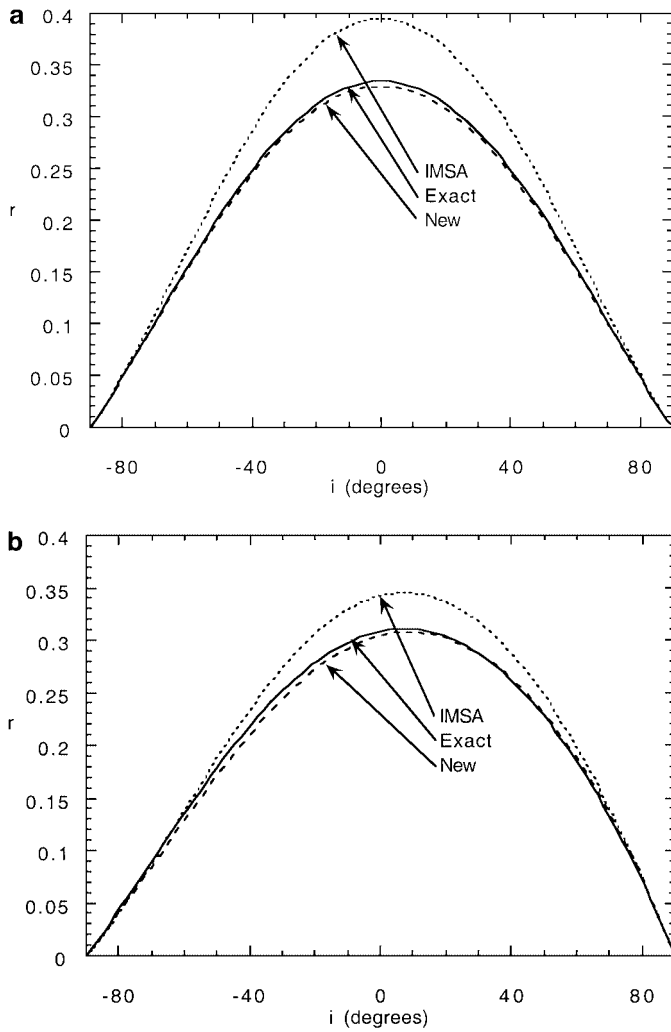The first-order Legendre polynomial expansion of $p(g)$ is

$$p(g) = 1 + b\cos g.$$

FIG. 4. Same as Fig. 3 but for $p(g) = 1 + \cos g$.

Then the only nonzero term is for $n = 1$, for which $A_1 = -1/2$, so that $P(i) = 1 - (b/2)\cos i$, $P(e) = 1 - (b/2)b\cos e$, and $\mathcal{P} = 1 - b/4$. This case is plotted in Fig. 4 for $b = +1$ and $w = 1$ and in Fig. 5 for $b = -1$ and $w = 1$ for the IMSA model, the improved model, and the exact model calculated using the tables in Chandrasekhar (1960).

Rayleigh Scatterers

For Rayleigh scatterers,

$$p(g) = \frac{3}{4}(1 + \cos^2 g) = \frac{3}{4}\left[1 + \frac{2P_2(\cos g) + 1}{3}\right]$$

$$= 1 + \frac{1}{2}P_2(\cos g).$$

Then only b_2 is nonzero. But $A_2 = 0$, so $P(i) = P(e) = \mathcal{P} = 1$. This case is plotted in Fig. 6 for $w = 1$, where the values from the tables in Chandrasekhar (1960) have been used for the exact model.

Single Henyey–Greenstein Function

The single Henyey–Greenstein function is

$$p(g) = \frac{1 - \xi^2}{(1 + 2\xi \cos g + \xi^2)^{3/2}}.$$

The parameter $\xi = \langle\cos\theta\rangle = -\langle\cos g\rangle$, $\theta = \pi - g$ is the scattering angle, and the angular brackets denote the average value over the range of angle between 0 and π. Expanding $p(g)$ in a Legendre polynomial series gives

$$p(g) = 1 + \sum_{n=1}^{\infty}(2n + 1)(-\xi)^n P_n(\cos g).$$

Hence, $b_n = (2n + 1)(-\xi)^n$.

An isolated particle that is large compared to the wavelength is strongly forward scattering because of the diffraction of light around it, so that ξ has a value close to 1.00. However, when the particle is close to other particles in a regolith the diffraction peak no longer exists (Hapke 1999), and for most particles
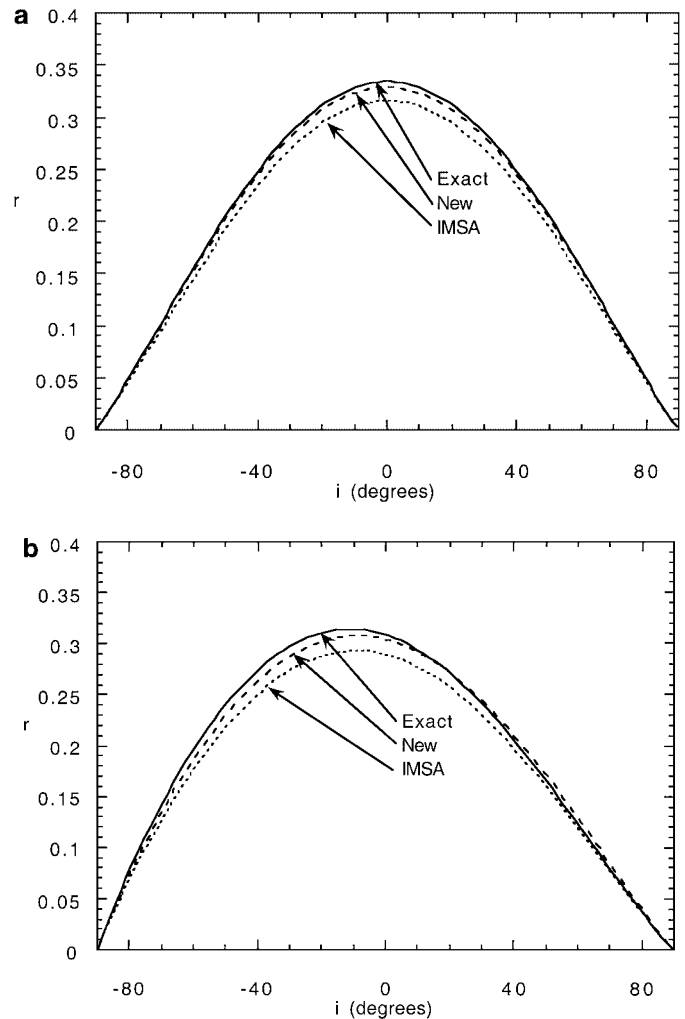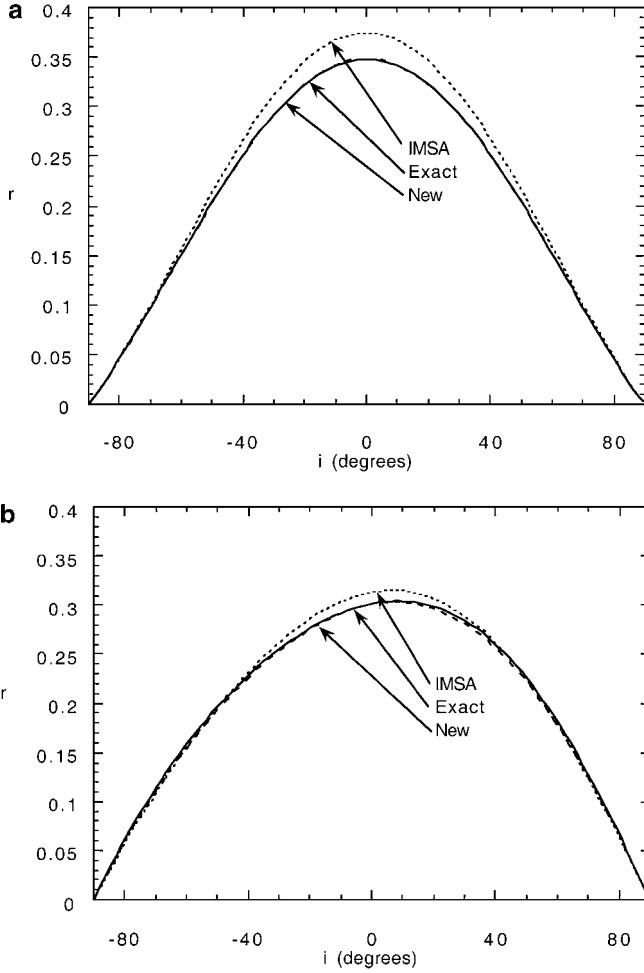

FIG. 5. Same as Fig. 3 but for $p(g) = 1 - \cos g$.

FIG. 6. Same as Fig. 3 but for Rayleigh scatterers ($p(g) = (3/4)(1 + \cos^2 g)$).

$\xi < \sim 0.6$ (McGuire and Hapke 1995). The reflectance of a medium of Henyey–Greenstein scatterers with $w = 1.00$ and $\xi = 0.6$ is plotted in Fig. 7. The exact values were calculated using the DISORT program of Stamnes *et al.* (1988).

Double Henyey–Greenstein Function

Most particle scattering functions have both a forward and a backward scattering lobe and hence are better described by a double Henyey–Greenstein function,

$$p(g) = \frac{1+c}{2} \frac{1-\xi_1^2}{\left(1+2\xi_1 \cos g + \xi_1^2\right)^{3/2}}$$
$$+ \frac{1-c}{2} \frac{1-\xi_2^2}{\left(1-2\xi_2 \cos g + \xi_2^2\right)^{3/2}}.$$

This requires specifying three parameters. However, in many cases of interest the scattering function can be represented to sufficient accuracy by a two-parameter function in which $\xi_1 = \xi_2 = \xi$ (McGuire and Hapke 1995, Hartmann and Domingue

1998). Therefore only the two-parameter function will be considered here. Then $p(g)$ is

$$p(g) = \frac{1+c}{2} \frac{1-\xi^2}{(1+2\xi \cos g + \xi^2)^{3/2}}$$
$$+ \frac{1-c}{2} \frac{1-\xi^2}{(1-2\xi \cos g + \xi^2)^{3/2}}$$
$$= \frac{1+c}{2}\left[1 + \sum_{n=1}^{\infty}(2n+1)(-\xi)^n P_n(\cos g)\right]$$
$$+ \frac{1-c}{2}\left[1 + \sum_{n=1}^{\infty}(2n+1)\xi^n P_n(\cos g)\right]$$
$$= 1 + \sum_{n=2,\text{even}}^{\infty}(2n+1)\xi^n P_n(\cos g)$$
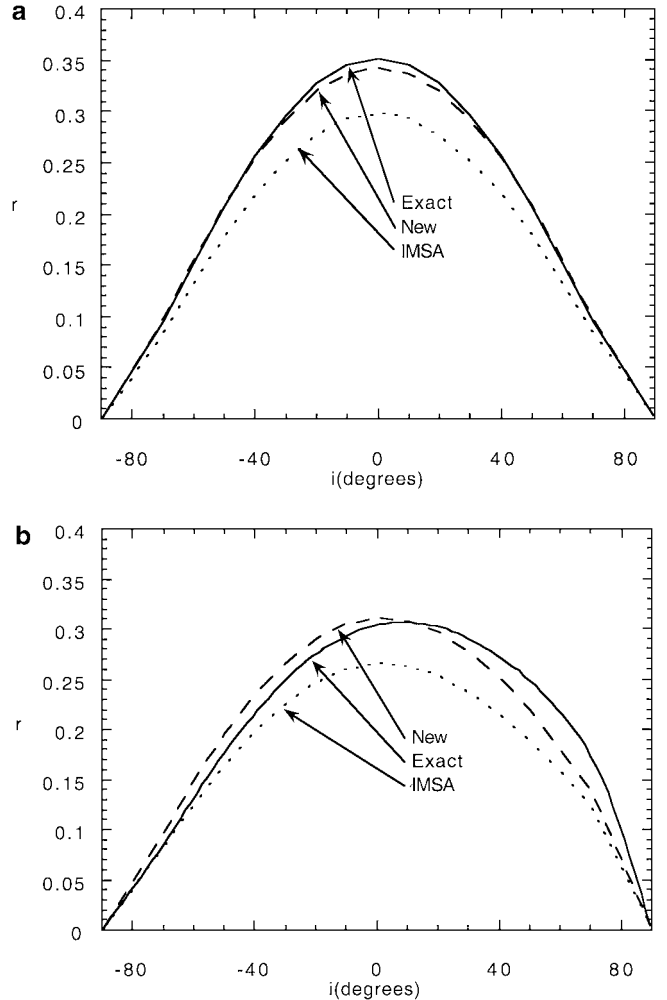$$- c\sum_{n=1,\text{odd}}^{\infty}(2n+1)\xi^n P_n(\cos g).$$

FIG. 7. Same as Fig. 3 but for Henyey–Greenstein scatterers with $\xi = 0.6$.

Since the even-n terms do not contribute, the only nonzero terms in (23)–(25) have

$$b_n = c(2n + 1)\xi^n,$$

where n is an odd integer.

6. IMPROVEMENT 3: THE COHERENT BACKSCATTER OPPOSITION EFFECT

Discussion

Two major mechanisms contribute to the opposition effect, shadow-hiding and coherent backscatter. The shadow-hiding opposition effect (SHOE) is caused by the fact that the shadow cast by one particle of the medium on another can be seen at all angles except zero phase, when each particle hides its own shadow, causing a relatively broad surge in brightness at small phase angles. The SHOE involves only the singly scattered rays. The coherent backscatter opposition effect (CBOE) results from the fact that portions of waves traveling in opposite directions along the same multiply scattered paths within a scattering medium interfere constructively with each other as they exit the medium near zero phase and cause a relative peak in brightness there. The CBOE can act on both the singly scattered and multiply scattered light. That the CBOE acts on all the light, and not just on the multiply scattered component, as is commonly believed, was first recognized by Helfenstein *et al.* (1997) in their analysis of the lunar opposition effect.

To understand why the SHOE acts only on the singly scattered light while the CBOE involves all the light, it is necessary to discuss the detailed processes that can occur when light is scattered from a complex medium like a planetary regolith. The light that is scattered at angles away from zero phase, which will be referred to as the continuum radiance, can be described by the equation of radiative transfer (Hapke 1993). The radiative transfer equation is a form of the diffusion equation, in which the light is treated as a series of waves (or in the geometric approximation, as rays) diffusing through the medium. A scattering event is considered to result from the interaction of a wave with a particle as a whole, and multiple scatterings are considered to occur only between entire particles. If the particle is complex because of inclusions, voids, or surface irregularities, these are accounted for by their effect on $p(g)$ (Hapke 1996, 1999). However, in theories of the opposition effect a scattering is any event that changes the direction of a photon. The event must be treated as if it occurred at a point and, thus, involves only a small portion of a particle. Hence, in models of the opposition effect in a medium consisting of large complex particles, multiple scatterings can occur between different parts of a single particle as well as between particles. Shkuratov and Helfenstein (2001) also have emphasized the importance of subparticle complexity.

In the SHOE a ray of light seen by a detector after scattering from a particle embedded in a particulate medium has been exponentially attenuated twice, once on the way in and once on
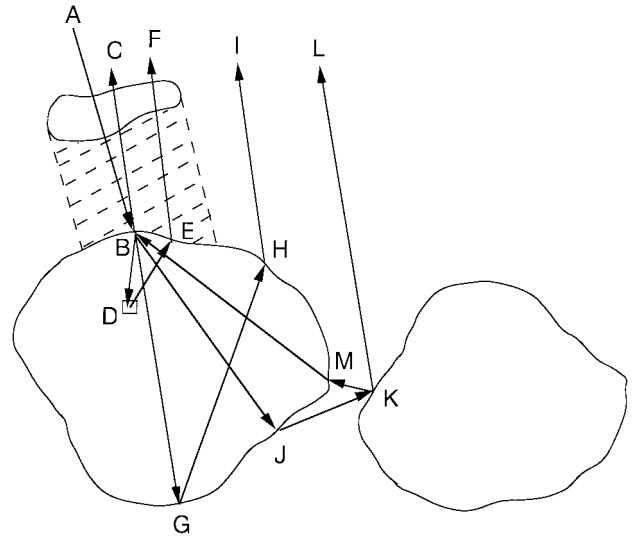

FIG. 8. Schematic diagram showing some of the wavepaths involved in the SHOE and CBOE.

the way out, except in the backscatter direction. For rays that are scattered back toward the source, the incident ray has, in effect, preselected an open path, so that backscattered rays can escape unattenuated. This gives rise to the SHOE peak. However, this is true only for rays that leave the particle close to the same point at which the incident ray encountered the particle, such as rays that are specularly reflected from the surface or scattered by a subsurface imperfection close to the entry point. Typical rays are shown schematically in Fig. 8 as ABC and ABDEF. In Fig. 8 the cross-hatched area is intended to denote schematically the clear volume that has been preselected by ray AB, and the square D denotes an imperfection such as an internal scatterer or a surface scatterer located close to point B.

Rays that are refracted into the particle and then leave it from a point located some distance away from the entry point, such as ray ABGHI, have a finite probability of being blocked, even if they are headed in the direction of the source. Hence, only part of the light backscattered by a particle contributes to the SHOE peak. A multiply scattered ray such as ABJKL will be too far from the preselected clear path to avoid being partially blocked and will not contribute. A ray such as ABJKMBC will contribute to the peak, but not only does such a ray scatter twice off of the first particle, but the second exit point must be very close to the initial entry point B. The fraction of rays that follow such restricted paths compared to all of the other multiply scattered rays is assumed to be so small that these rays can be neglected. Thus, the SHOE multiplies only the single-scattering term.

To contribute to the CBOE not only must a ray be scattered more than once, but the point at which it is first scattered within the medium must be separated by a finite distance from the last point from which it is scattered as it leaves the medium. The closer together the two points are, the larger the range of phase angles at which constructive interference occurs. If the two points coincide, such as ray ABJKMBC, waves that travel

in opposite directions over the same path will be in phase for all phase angles so that the coherently scattered light will contribute to the continuum intensity, and no discrete CBOE peak will occur. In media made up of large, physically complex particles the entrance and exit points can be located on the same particle, as is the case for rays ABDEF and ABGHI. If a large fraction of such backscattered rays have end points that are separated by only a few wavelengths the CBOE peak can be several degrees wide. Note that some of the rays that are treated in the radiative transfer equation as singly scattered contribute to the CBOE, including some of the rays that also contribute to the SHOE, as well as those that the equation treats as multiply scattered, such as ray ABJKL. Thus, the CBOE multiplies the singly scattered component of the scattered light, including the SHOE, as well as the multiply scattered component.

This discussion explains several puzzling properties of the CBOE found by laboratory studies of media composed of complex particles: Nelson *et al.* (2000) experimentally found little dependence of the angular width of the CBOE on particle size; low albedo materials, such as the lunar regolith, have strong CBOEs (Hapke *et al.* 1993, 1998; Helfenstein *et al.* 1997); and media of particles much larger than the wavelength have CBOEs that are broad enough to be readily observable (Nelson *et al.* 2000). These results are contrary to theoretical expectations based on models of media composed of simple, independently scattering spheres (Mishchenko 1992).

Theoretically, the maximum amount by which either the SHOE or the CBOE separately can increase the brightness at zero phase over its continuum value is a factor of 2. However, the preceeding discussion shows that there are several phenomena that reduce this value. An additional reason results from light being a vector quantity with two components of polarization. Scatterings in which the component of linear polarization is preserved contribute more strongly to both opposition effects than scatterings in which the polarization is reversed. Unfortunately, the amplitudes of the opposition effects cannot be calculated in general. The only known way to describe them with any degree of rigor would be to carry out a Monte Carlo scattering calculation, while keeping track of all shadows and the phases of all waves in the medium. Such a calculation is impractical for most applications. For this reason, the amplitudes of the opposition effects are left as model parameters to be empirically fitted.

The Shadow-Hiding Opposition Effect

The SHOE is discussed quantitatively in Hapke (1986, 1993). The equations derived there are retained in the new model. The surge is described by multiplying the single-scattering term, represented by $p(g)$ in $L(i, e, g)$, by the function

$$B_{SH}(g) = 1 + B_{S0}B_S(g), \qquad (28)$$

where B_{S0} is the amplitude of the SHOE and is constrained by physical considerations to be ≤ 1 and

$$B_S(g) = [1 + (1/h_S)\tan(g/2)]^{-1}, \qquad (29)$$

where

$$h_s = -E\langle a\rangle \ln(1-\phi)/2\phi, \qquad (30)$$

E is the extinction coefficient in the medium, $\langle a\rangle$ is the mean particle radius, and ϕ is the filling factor.

The function $B_S(g)$ has the following properties: $B_S(0) = 1$; at $g = 0$ the slope $dB_S/dg = -1/2h_S$; the half width at half maximum (HWHM) occurs when $(1/h_S)\tan(g/2) = 1$ so that the SHOE HWHM is approximately

$$g_{S(1/2)} = 2h_S. \qquad (31)$$

The Coherent Backscatter Opposition Effect

It must first be emphasized that no rigorous theory for the CBOE in a medium of large complex particles presently exists. Akkermans *et al.* (1988) have discussed the CBOE in terms of a model based on a random walk by photons in a scattering half-space. We choose their formulation because it predicts a quantitative relation between the HWHM and the transport mean free path that has been experimentally verified by Van Albada *et al.* (1990) for colloidal suspensions of latex spheres over a wide variety of sizes and separations. It also gives a good fit to the measured reflectances of alumina abrasive powders (Nelson *et al.* 2000). We adapt the Akkermans *et al.* equation with a minor modification and describe the CBOE by multiplying the entire reflectance by the function

$$B_{CB}(g) = 1 + B_{C0}B_C(g), \qquad (32)$$

where B_{C0} is the amplitude of the CBOE and is constrained by physical considerations to be ≤ 1,

$$B_C(g) = \frac{1 + \frac{1 - e^{-(1/h_C)\tan(g/2)}}{(1/h_C)\tan(g/2)}}{2[1 + (1/h_C)\tan(g/2)]^2}, \qquad (33)$$

$$h_C = \lambda/4\pi\Lambda, \qquad (34)$$

λ is the wavelength, and Λ is the transport mean free path in the medium.

The transport mean free path may be thought of as the mean distance a photon travels in the medium before its direction is changed by a large angle, say 1 radian. The conventional expression for Λ is

$$\Lambda = [n\sigma Q_S(1 - \langle\cos\theta\rangle)]^{-1}, \qquad (35)$$

where n is the number of particles per unit volume, σ is the mean particle cross-sectional area, Q_S is the mean particle scattering efficiency, and $\langle\cos\theta\rangle$ is the mean cosine of the scattering angle. However, in view of the general discussion in this section, Eq. (35) must be applied with considerable care. In media of large complex particles, Λ is heavily weighted by the effects of internal and surface scattering inhomogeneities.

The function $B_C(g)$ has the following properties: $B_C(0) = 1$; at $g = 0$, $dB_C/dg = -9/16\,h_C$; the HWHM occurs when $(1/h_C)\tan(g/2) = 0.36$, so that the CBOE HWHM is approximately

$$g_{C(1/2)} = 0.36\,\lambda/2\pi\,\Lambda. \qquad (36)$$

Shkuratov and Helfenstein (2001) have suggested that at small phase angles, instead of Eq. (33), a function of the form

$$B_C(g) = 1 + \frac{1}{2\sqrt{1+(Kg)^2}}, \qquad (37)$$

where K is a constant that depends on the medium and the viewing conditions, be used. A major difference between the two is that Eq. (33) comes to a cusp at $g = 0$, whereas Eq. (37) is flat there. However, there is no indication of a flattening of the CBOE peak in the experimental data on powders of either high (Nelson *et al.* 2000) or low (Hapke *et al.* 1998) albedo. Hence, Eq. (33) is preferred.

The opposition effect functions $B_S(g)$ and $B_C(g)$ are plotted in Fig. 9. Rather than plot these quantities versus g, to better compare the two functions we plot $B_S(g)$ against the quantity $z = (1/h_S)\tan(g/2)$ and $B_C(g)$ against $z = 0.36(1/h_C)\tan(g/2)$. When shown in this way the initial values and the half-power points of the two curves coincide. As g increases, the two functions are virtually indistinguishable out to the half-power angles, but thereafter $B_C(g)$ falls off more rapidly than $B_S(g)$.

Unfortunately, including the CBOE adds two more parameters to be fitted by the model. However, these parameters affect the reflectance only at small phase angles, where frequently observational data are sparse. The similarity in the shapes of the functions plotted in Fig. 9 shows that it would be extremely difficult to distinguish SHOE from CBOE on the basis of shape alone without other information such as dependence on albedo, wavelength, or circular polarization (Hapke 1990). Hence, in
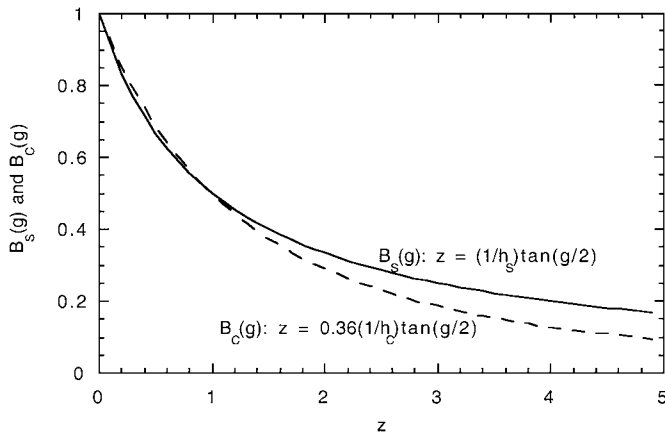

FIG. 9. The SHOE $B_S(z)$ and CBOE $B_C(z)$ functions. The arguments of the functions have been separately scaled to make the half-power points of the two curves coincide. For the SHOE function, $B_S(g)$ has been plotted against the quantity $z = (1/h_S)\tan(g/2)$ and for the CBOE function, $B_C(g)$ has been plotted against $z = 0.36(1/h_C)\tan(g/2)$.

many applications it may be sufficient to describe the opposition effect by simply multiplying the total background reflectance, Eq. (1) or (18), by an expression of the form of Eqs. (28) and (29), without trying to explicitly separate the SHOE and CBOE.

7. THE NEW MODEL

Following the suggestion by Helfenstein *et al.* (1997) and combining the results of Sections 4–6 gives the final expression for the new model,

$$r(i, e, g) = \frac{w}{4\pi}\frac{\mu_o}{\mu_o+\mu}[p(g)B_{SH}(g)+M(\mu_o, \mu)]B_{CB}(g), \quad (38)$$

where $M(\mu_o, \mu)$, $B_{SH}(g)$, and $B_{CB}(g)$ are given by Eqs. (17), (29), and (32), respectively, and Eq. (13) is used for the H-functions in $M(\mu_o, \mu)$.

8. THE DIRECTIONAL-HEMISPHERICAL REFLECTANCE

The directional-hemispherical reflectance r_h, also known as the hemispherical albedo and plane albedo, is derived in this section. It is of interest because it is usually the type of reflectance measured with an integrating sphere, and it is also the albedo that is needed for thermal modeling of planetary surfaces illuminated by sunlight. As in the IMSA model, it is assumed that the light scattered by the opposition effect can be ignored because the angular width of the peak is so narrow. The general expression for the hemispherical albedo is (Hapke 1993)

$$r_h = \frac{1}{\mu_o} \int\limits_{e=0}^{\pi/2} \int\limits_{\varphi=0}^{2\pi} r(i, e, g)\mu \sin e\, de\, d\varphi$$

$$= \frac{w}{4\pi} \int\limits_{e=0}^{\pi/2} \int\limits_{\varphi=0}^{2\pi} \frac{\mu}{\mu_o + \mu} L(i, e, g)\sin e\, de\, d\varphi. \qquad (39)$$

Using the formalism developed in Section 5 for the case where $p(g)$ is expressed as a Legendre polynomial series, and remembering that the integral of $\cos m\varphi\, d\varphi$ over the interval from 0 to 2π is 0, after straightforward algebra, Eq. (39) can put into the form

$$r_h = \frac{w}{2} \int\limits_0^1 \frac{\mu}{\mu_o + \mu} H(\mu_o)H(\mu)\, d\mu + \sum_{n=1}^{\infty} b_n\{P_n(\mu_o)$$

$$+ A_n[H(\mu_o) - 1]\} \left[\frac{w}{2} \int\limits_0^1 \frac{\mu}{\mu_o + \mu} P_n(\mu)\, d\mu \right.$$

$$\left. + A_n\frac{w}{2} \int\limits_0^1 \frac{\mu}{\mu_o + \mu} H(\mu)\, d\mu - A_n\frac{w}{2} \int\limits_0^1 \frac{\mu}{\mu_o + \mu}\, d\mu \right] \quad (40)$$

The first integral on the right hand side of Eq. (40) can be evaluated using the identiy $\mu/(\mu_o + \mu) = 1 - \mu_o/(\mu_o + \mu)$

together with Eq. (9), the defining equation for the H-functions. This gives

$$\frac{w}{2} \int_0^1 \frac{\mu}{\mu_o + \mu} H(\mu_o) H(\mu) \, d\mu = 1 - \gamma H(\mu_o). \qquad (41a)$$

Because $P_n(\mu)$ can be expressed as a sum of powers of μ, the first integral inside the square brackets under the summation in the right side of (40) consists of terms of the form

$$\frac{w}{2} \int_0^1 \frac{\mu^j}{\mu_o + \mu} \, d\mu,$$

where j is an integer; these are listed in standard tables of integrals and can be evaluated for any values of n and j. The second integral inside the square brackets can be evaluated using the previously mentioned identity together with Eq. (9) to give

$$A_n \frac{w}{2} \int_0^1 \frac{\mu}{\mu_o + \mu} H(\mu) \, d\mu = A_n \left[\frac{1}{H(\mu_o)} - \gamma \right]. \qquad (41b)$$

The third integral inside the square brackets is

$$A_n \frac{w}{2} \int_0^1 \frac{\mu}{\mu_o + \mu} \, d\mu = A_n \frac{w}{2} \left[1 - \mu_o \ln \frac{1 + \mu_o}{\mu_o} \right]. \qquad (41c)$$

Thus the hemispherical albedo is

$$r_h = 1 - \gamma H(\mu_o) + \sum_{n=1}^{\infty} b_n \{ P_n(\mu_o) + A_n [H(\mu_o) - 1] \}$$

$$\times \left\{ \frac{w}{2} \int_0^1 \frac{\mu}{\mu_o + \mu} P_n(\mu) \, d\mu + A_n \left[\frac{1}{H(\mu_o)} - \gamma \right] \right.$$

$$\left. - A_n \frac{w}{2} \left[1 - \mu_o \ln \frac{1 + \mu_o}{\mu_o} \right] \right\}. \qquad (42)$$

Equation (42) will be evaluated explicitly for $p(g) = 1 + b_1 \cos g$. For this case, $b_n = 0$ for $n > 1$, $A_1 = -1/2$, $P_1(\mu_o) = \mu_o$, and $P_1(\mu) = \mu$, so that

$$\frac{w}{2} \int_0^1 \frac{\mu}{\mu_o + \mu} P_1(\mu) \, d\mu = \frac{w}{2} \int_0^1 \frac{\mu^2}{\mu_o + \mu} \, d\mu$$

$$= \frac{w}{2} \left[\frac{1}{2} - \mu_o + \mu_o^2 \ln \frac{1 + \mu_o}{\mu_o} \right].$$

Hence,

$$r_h = 1 - \gamma H(\mu_o) + b_1 \left\{ \mu_o - \frac{1}{2} [H(\mu_o) - 1] \right\}$$

$$\times \left\{ \frac{w}{2} \left[\frac{1}{2} - \mu_o + \mu_o^2 \ln \frac{1 + \mu_o}{\mu_o} \right] + \frac{1}{2} \left[\frac{1}{H(\mu_o)} - \gamma \right] \right.$$

$$\left. - \frac{w}{4} \left[1 - \mu_o \ln \frac{1 + \mu_o}{\mu_o} \right] \right\}. \qquad (43)$$

If the particles are isotropic scatterers, $b_n = 0$ and $r_h = 1 - \gamma H(\mu_o)$, a result that has been previously derived (Hapke 1993). For the case $w = 1$ and $\mu_o = 1$, Eq. (43) gives $r_h = 1 + 0.0088 b_1$. The errors in the improved model may be judged from the fact that, when $w = 1$, all the incident light must be scattered back out so that $r_h = 1$ for any value of μ_o. Since $|b_1| \le 1$, the error is <1%.

9. SUMMARY

The improved model is given by Eq. (38) and consists of three modifications:

1. A more accurate analytic approximation to the Ambartsumian–Chandrasekhar H-functions for isotropic scatterers is given by Eq. (13).

2. An expression for the bidirectional reflectance that is more accurate than the IMSA model when the scatterers are anisotropic is given by Eqs. (15)–(18). The parameters in these expressions have been evaluated for Legendre polynomial particle scattering functions, including those cases when it is convenient to express the Henyey–Greenstein function as a Legendre polynomial series.

3. Coherent backscattering has been incorporated. An expression for the CBOE is given by Eq. (32).

A difficulty with the practical application of a model of this form was pointed out by Helfenstein *et al.* (1997) and was also discussed by Hapke *et al.* (1998). In attempting to retrieve parameters there are two possible solutions: one with a narrow CBOE and wide SHOE and the other with the reverse of this. Physical considerations suggest that the solution with the narrow CBOE is most likely to be correct.

This paper has ignored macroscopic roughness. The effects of roughness on a scale large compared to the particle size may be corrected for using the formalism in Hapke (1984, 1993), which was derived for any general reflectance function.

ACKNOWLEDGMENTS

REFERENCES

Akkermans, E., E. Wolf, R. Maynard, and G. Maret 1988. Theoretical study of the coherent backscattering of light by disordered media. *J. Phys. France* **49**, 77–98.

Ambartsumian, V. 1958. *Theoretical Astrophysics*. Pergamon, New York.

Chandrasekhar, S. 1960. *Radiative Transfer*. Dover, New York.

Hapke, B. 1981. Bidirectional reflectance spectroscopy. 1. Theory. *J. Geophys. Res.* **86**, 3039–3054.

Hapke, B. 1984. Bidirectional reflectance spectroscopy. 3. Correction for macroscopic roughness. *Icarus* **59**, 41–59.

Hapke, B. 1986. Bidirectional reflectance spectroscopy. 4. The extinction coefficient and the opposition effect. *Icarus* **67**, 264–280.

Hapke, B. 1990. Coherent backscatter and the radar characteristics of outer Solar System planetary satellites. *Icarus* **88**, 407–417.

Hapke, B. 1993. *Theory of Reflectance and Emitance Spectroscopy*. Cambridge Univ. Press, Cambridge, UK.

Hapke, B. 1996. Are planetary regolith particles back scattering? Response to a paper by M. Mishchenko. *J. Quant. Spectrosc. Radiat. Transfer* **55**, 837–848.

Hapke, B. 1999. Scattering and diffraction of light by particles in planetary regoliths. *J. Quant. Spectrosc. Radiat. Transfer* **61**, 565–581.

Hapke, B., R. Nelson, and W. Smythe 1993. The opposition effect of the Moon: The contribution of coherent backscattering. *Science* **260**, 509–511.

Hapke, B., R. Nelson, and W. Smythe 1998. The opposition effect of the Moon: Coherent backscatter and shadow hiding. *Icarus* **133**, 89–97.

Hartman, B., and D. Domingue 1998. Scattering of light by individual particles and the implications for models of planetary surfaces. *Icarus* **131**, 421–448.

Helfenstein, P., J. Veverka, and J. Hillier 1997. The lunar opposition effect: A test of alternative models. *Icarus* **128**, 2–14.

Jahnke, E., and F. Emde 1945. *Tables of Functions*. Dover, New York.

Kuga, Y., and A. Ishimaru, 1984. Retroreflectance from a dense distribution of spherical particles. *J. Opt. Soc. Am. A* **1**, 831–835.

McGuire, A., and B. Hapke 1995. An experimental study of light scattering by large, irregular particles. *Icarus* **113**, 134–155.

Mishchenko, M. 1992. The angular width of the coherent backscatter opposition effect: An application to icy outer planet satellites. *Astrophys. Space Sci.* **194**, 327–333.

Mischenko, M., and J. Dlugaach 1992. Can weak localization of photons explain the opposition effect of Saturn's rings? *Mon. Not. R. Astron. Soc.* **254**, 15–18.

Muinonen, K. 1990. *Light Scattering by Inhomogeneous Media: Backward Enhancement and Reversal of Linear Polarization*. Ph.D. thesis, University of Helsinki.

Nelson, R., B. Hapke, W. Smythe, and L. Horn 1998. Phase curves of selected particulate materials: The contribution of coherent backscattering to the opposition surge. *Icarus* **131**, 223–230.

Nelson, R., B. Hapke, W. Smythe, and L. Spilker 2000. The opposition effect in simulated planetary regoliths. Reflectance and circular polarization ratio change at small phase angle. *Icarus* **147**, 545–558.

Shkuratov, Y. 1988. A diffraction mechanism for the formation of the opposition effect of the brightness of surfaces having a complex structure. *Kinem. Fiz. Nebes. Tel.* **4**, 33–39.

Shkuratov, Y., and P. Helfenstein 2001. The opposition effect and the quasi-fractal structure of regolith. 1. Theory. *Icarus* **152**, 96–116.

Sobolev, V. 1975. *Light Scattering in Planetary Atmospheres*. Pergamon, New York.

Stamnes, K., S. Tsay, W. Wiscombe, and K. Jayaweera 1988. Numerically stable algorithm for discrete-ordinate-method radiative transfer in multiple scattering and emitting layered media. *Appl. Opt.* **27**, 2502–2509. (Information for downloading the DISORT program via the Internet is *available at* wiscombe@climate.gsfc.nasa.gov.).

Van Albada, M., M. Van der Mark, and A. Lagendijk 1990. Experiments on weak localization of light and their interpretation. In *Scattering and Localization of Classical Waves in Random Media* (P. Sheng, Ed.), pp. 97–136. World Scientific, Teaneck, NJ.